Articles
doi.org/10.1002/batt.202100056

Chemistry Europe
European Chemical Societies Publishing

The Impact of the C-Rate on Gassing During Formation of NMC622 II Graphite Lithium-Ion Battery Cells

Marco Leißing,[a] Fabian Horsthemke,[a] Simon Wiemers-Meyer,[a] Martin Winter,[a, b] Philip Niehoff,*[a] and Sascha Nowak*[a]

Formation is considered a cost and time intensive production step in industrial production of lithium-ion batteries (LIBs). One solution for improvement is an acceleration of the formation step by applying higher C-rates. In this study, formation protocols with up to 2 C were applied to $LiNi_{0.6}Mn_{0.2}Co_{0.2}O_2$ (NMC622) II graphite pouch cells with a nominal capacity of 5 Ah. The formation protocols utilizing higher C-rates result in a decrease in overall formation time, but also in increased gassing due to additional electrolyte decomposition. The resulting gas phase was quantitatively determined using gas chromatography-barrier discharge ionization detection (GC-BID) and with regard to gas volume by making use of the Archimedes principle. Main formation gases in these cells were identified as CO and C_2H_4. Increased C-rates altered certain decomposition reactions. Especially the CO evolution was increased. Nevertheless, gassing was smallest for 0.1 C and increased with lower and higher C-rate. In case of too low C-rates hydrogen was identified as the main formation gas. However, higher gassing was not correlated with higher capacity loss during formation. Furthermore, the dependence of the C-rate on gassing was found to be dependent on the graphite material.

1. Introduction

During the first charge and discharge cycles of a lithium-ion battery (LIB), the so-called formation (cycles), the electrolyte decomposes mostly on the negative electrode, where electronically non-conducting components precipitate to a film called solid electrolyte interphase (SEI). In literature some studies address the cathode electrolyte interphase (CEI) which is forming at the positive electrode. However, SEI formation and composition have been traditionally addressed in more detail in research.[1–8] However, both SEI and CEI formation are scientifically not well understood. The interphases formation is typically performed at C-rates of 0.05 C which results in a formation time of days to weeks. This makes the formation to a time and cost-consuming step in the industrial battery cell production[9,10] Accelerating this process step has the potential to significantly decrease production costs and time.[10,11] During electrolyte decomposition and interphase formation gaseous decomposition products evolve. The cell setup and electrochemical conditions have a strong impact on the quantity and composition of these mostly flammable formation gases.[12–14] Therefore, optimization of the formation considering the gassing is an important area of research.

The major components of a LIB cell are the two electrodes, commonly graphite as negative electrode material and a lithium transition metal oxide as positive electrode material, both are electronically isolated by an electrolyte-soaked separator.[15] The electrolyte is needed to enable the transfer of ions, in particular Li-ions between the electrodes. Mixtures of cyclic and linear organic carbonates like ethylene carbonate (EC) and ethyl methyl carbonate (EMC) are commonly used electrolyte solvents today. Lithium hexafluorophosphate ($LiPF_6$) is the most commonly used conducting salt in commercial LIBs due to its overall properties.[16–18]

During the first charge and discharge step of the battery, a protective layer - SEI - forms on the surface of the negative electrode since the used electrolyte is not stable at low electrode potentials (<1.4 V vs. Li^+/Li) at the negative electrode. Hence, the SEI is composed of degradation products, which are generated *via* electrochemical reduction and precipitation on the surface.[19,20] Examples for solid inorganic and organic precipitates are Li_2O, Li_2CO_3, LiF, $ROCO_2Li$ and a variety of polymers.[20–23] Due to an electronically insulating effect, the SEI protects the electrolyte from further degradation and the graphite from co-intercalation of electrolyte and solvent molecules which would lead to exfoliation of graphite. Despite the electronic isolation, the SEI provides permeability for Li-ions to ensure an intercalation and deintercalation in the negative electrode.[19] Analogous to the SEI, the CEI can form on the cathode from oxidative decomposition products. However, high electrolyte oxidation potential (>4.5 V vs. Li^+/Li) leading to the evolution of gas products *e.g.* CO or CO_2. Since these

[a] M. Leißing, Dr. F. Horsthemke, Dr. S. Wiemers-Meyer, Prof. M. Winter, Dr. P. Niehoff, Dr. S. Nowak
University of Münster
MEET Battery Research Center
Corrensstraße 46, 48149 Münster, Germany
E-mail: sascha.nowak@uni-muenster.de
philip.niehoff@uni-muenster.de
[b] Prof. M. Winter
Helmholtz-Institute Münster
IEK-12, Forschungszentrum Jülich
Corrensstraße 46, 48149 Münster, Germany

potentials are generally not reached, the direct contribution to the amount of formation gas is limited. Nevertheless, cross talk phenomena between the electrodes and the formation of intermediates with lower oxidation potential have to be considered.[24,25] This can be done using an experimental, two compartment cell setup which is the natural next step of our studies.[25]

Since the interphase formation is time consuming, there is great interest in accelerating this process, e.g. by applying higher C-rates. Nevertheless, this has to be balanced with quality, safety and performance of the cell. Hence, deeper understanding of the chemical and electrochemical reactions at the electrode-electrolyte interface is a key to improve the overall battery performance.[10,12,26–32] Due to the decomposition of the electrolyte during formation, the interphase formation is accompanied by the evolution of gaseous components. This gas evolution is particularly visible in pouch type LIB cells and the amount can be determined *via* the Archimedes principle.[33] The gassing depends on the electrode materials, electrolytes, additives and cut-off voltages. For different $LiNi_xMn_yCo_zO_2$ (NMC; $x+y+z=1$) materials, graphite and an EC based electrolyte gas amounts between 1.5 mL Ah^{-1} and 7.0 mL Ah^{-1} were described in literature.[34–36] Not only the overall gas volume, but also the qualitative and quantitative composition of the formation gas is of interest. Gases like H_2, CO, CO_2, CH_4, C_2H_4 and C_2H_6 were determined during or after formation. Not only the formation gas volume but also the composition of these gases can vary in LIBs. According to literature data H_2, CO, CO_2 and/or C_2H_4 were found to be the highest concentrated gases in the gas phase after formation.[37–42] Since these results differ greatly, it is from great interest to investigate factors influencing certain decomposition reactions and to clarify possible reaction pathways leading to a certain gas component. Understanding and controlling gas formation reactions related to SEI formation is a big step towards safety and performance of LIBs.

In this study we investigated the hypothesis that the gassing is a measure of incomplete interphase formation. The electrolyte decomposes especially on the anode side if the interphase is not completely formed. Here, the influence of C-rates between 0.05 C to 2 C during formation on the gas volume and composition in $LiNi_{0.6}Mn_{0.2}Co_{0.2}O_2$ (NMC622) II graphite cells was investigated. The findings were compared by investigating a 2nd graphite material.

Experimental Section

Cell Chemistry and Cell Preparation

NMC622 II graphite pouch cells with a nominal capacity of 5 Ah were assembled as follows. The electrode sheets and cells were produced at the MEET in-house battery line using a continuous coating and drying process followed by calendaring resulting in a porosity of ≈30%. The two-electrode cells according to Nölle *et al.*[43] were composed of 19 negative electrode (121×68 mm) and 18 positive electrode (119×66 mm) sheets. The latter comprised NMC622 (95 wt.%; BASF, Germany) as active material, conductive carbon Super C65 (2 wt.%; Imerys, France) and polyvinylidene difluoride (3 wt.%; Kureha, USA) as binder coated on both sides of a 15 μm Al foil (Nippon Foil, Japan). The negative electrode consisted of two different, commercially available, artificial graphite materials (G I; industrial supplier 1, 95 wt.%; G II; industrial supplier 2, 95 wt.%) as active material, conductive carbon Super C65 (0.5 wt.%; Imerys), carboxymethylcellulose (Walocel CRT 2000 PA, 3 wt.%; Chempoint, USA), and styrene-butadiene rubber (Lipaton SB 5521; Synthomer, United Kingdom) as binder coated on both sides of a 10 μm Cu foil (Nippon foil). The single sided mass loading of the positive and negative electrode was 13.5 mg cm^{-2} and 7.8 mg cm^{-2}, respectively. As separator, Mitsubishi OZ-S30 (30 μm; Mitsubishi Paper Mills Limited, Japan) with one sided ceramic coating was used. The stacking was carried out by Z-folding. Cells were filled with 27.5±0.1 g electrolyte, (equivalent of 1.6 times the pore volume of the dry cell). The electrolyte (Soulbrain, USA) consisted of EC and EMC in a ratio of 3:7 wt.%, 1.0 mol L^{-1} $LiPF_6$ and 2 wt.% of vinylene carbonate (VC). Following the cells were sealed under reduced pressure (−80 kPa, 20 s) and stored for wetting in a climate chamber (2 h at 20 °C).

Samples for liquid electrolyte measurements were extracted from 18650 cells. These cells were built with the same materials as described above. The preparation of the samples were conducted according to Horsthemke *et al.*[44] For the following investigations at least three cells were used to analyse the respective parameter and determine the standard deviation.

Electrochemical Formation

After wetting of the cells, one formation cycle was performed at 20 °C for each cell in a constant-current constant-voltage (CCCV) charging and constant-current (CC) discharging mode with 4.2 V and 3.0 V as terminating cell voltages. CCs were 0.25 A (0.05 C), 0.5 A (0.1 C), 1 A (0.2 C), 5 A (1 C) and 10 A (2 C), respectively. A constant-voltage (CV) step at 4.2 V was performed for 30 min.

After discharge, Archimedes and GC measurements were performed.

Gas Chromatography

All gas chromatography (GC) measurements were performed using a GC-2010 Plus system (Shimadzu, Germany). A PLOT gas separation column RT®-Msieve 5 A (30 m×0.32 mm×30 μm; Restek, Germany) in combination with a barrier discharge ionization (BID) detector (Shimadzu) was used for the quantification of permanent gases and hydrocarbons except CO_2. For CO_2 measurements, a packed RT®-ShinCarbon ST (80/100, 2.0 m×0.53 mm; Restek) was utilized and coupled to a thermal conductivity detector (TCD; Shimadzu) for quantification. Helium (purity 6.0; Westfalen, Germany) was used as carrier gas. Further settings and gas sampling were conducted according to a previous publication.[45]

The electrolyte quantification was done using a GC-flame ionization detector (GC-FID). Experiments were executed on a Clarus 600 (PerkinElmer, USA) and a Rxi®-5 ms (30 m×0.25 mm, 0.25 μm; Restek) diphenyl dimethyl polysiloxane (5%/95%) fused silica column. Further parameters and sample preparation were conducted according to Terborg *et al.*[46]

The gas phase of each cell was extracted and quantified three times by GC. The obtained values for the relative composition of each component were combined to form a mean value. The three mean values observed from each cell are further combined to a mean value. The resulting value and the standard deviation hence show the deviation between the gas composition of three different

cells. Lastly the relative composition was corrected with the total gas volume and the respective error.

Gas Volume Determination and Sampling

The weight of the pouch type cells in water was measured before and after the electrochemical treatment for the evaluation of the evolved gas volume. A setup introduced by Aiken *et al.* was used for these measurements.[36] The setup was modified for 5 Ah cells with a weight of ≈125 g (load cell: KD45 2 N; ME-Meßsysteme, Germany).

Sampling was performed using a 25 µL gas tight syringe. Samples of 5 and 20 µL were sampled from the gas bag of the pouch cell and injected manually into the GC-system. The sampling approach is a convenient method to transfer gases from the pouch cells into the GC-system with negligible contamination by air and less preparation in advance. In the first preparation step a septum was tightly glued on the gas bag of the pouch cell by use of silicone. Following, a sealed and evacuated cannula was pierced through the septum and then carefully through the outer layer of the pouch foil. The cannula provided a small headspace for sampling without contact to the liquid electrolyte in the cell.[45]

2. Results and Discussion

In order to get more insights into the dependency of formation time and electrolyte decomposition during SEI building, different C-rates were applied to NMC622 II graphite cells. The full cell setup should reflect all processes in the cell as realistically as possible on the level of a laboratory cell.

In Figure 1 the cell voltage over time is given for the different formation procedures. For the initial cycle a CC charge step to 4.2 V followed by a CV step for 30 min and a CC discharge to 3.0 V was applied to the cells. The charge and discharge current were adjusted to 0.05 C, 0.1 C, 0.2 C, 1 C and 2 C. The formation with 2 C leads to an overall formation time of 1.25 h and for the 1 C formation to 2.5 h. The 0.2 C formation takes 12 h, the 0.1 C formation 24 h and the 0.05 C formation

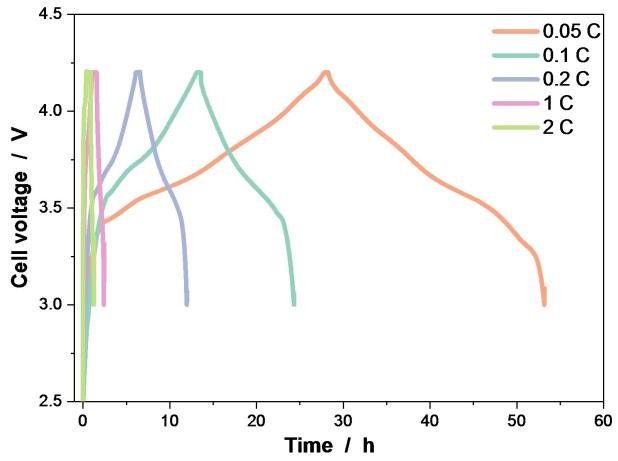

Figure 1. Cell voltage over time plotted for the formation cycle of NMC622IIgraphite cells. Different C-rates (0.05 C, 1.0 C, 0.2 C, 1 C, and 2 C) were applied.

53 h, respectively. It can be noticed that the experimental formation time does not correlate directly with the set C-rate and the calculated formation time. The experimental formation time is influenced by three factors: 1. The formation time was calculated with the nominal capacity C-rate which does only hold true after formation under certain cycling conditions. 2. The overpotentials are increasing with higher C-rate resulting in a lower SOC reached during charge and hence shortening the formation time. Furthermore, this can result in a smearing of the line shape. 3. Different amounts of side reactions during charge can lead to longer charging times than discharge times especially for the low C-rates.

In this paper, it was differentiated between two different processes leading to gas formation during the first charge and discharge of the battery cell. Gassing which originates from decomposition reactions forming SEI called specific gassing and gassing which is not associated with forming SEI called unspecific gassing. The specific gassing describes gases resulting from processes which consume Li to form the interphases, especially on the negative electrode. Unspecific gassing results from the direct decomposition of electrolyte or electrolyte crosstalk species without consumption of Li.

In general, it cannot be differentiated between certain gases resulting from specific or unspecific gassing since the reaction products are the same. Furthermore, these two processes can occur simultaneously which makes it even harder to distinguish between these processes. In theory at very low C-rate unspecific gassing should increase as it takes longer to build an effective SEI. The higher the C-rate becomes the lower the time where a potential high enough to decompose electrolyte is present, hence the unspecific gassing should decrease. In the following, the gassing during formation with different C-rates was investigated regarding the produced gas volume.

2.1. Gassing During Formation

Figure 2 shows the results of gas volume determination *via* Archimedes principle after formation. The gas volume was directly measured after discharge was completed and the cell voltage reached 3.0 V. The figure depicts, the C-rate alteration effects on the total gassing during formation. From 0.1 C (1.6 ± 0.2 mL) to 0.2 C (2.6 ± 0.6 mL), 1 C (5.2 ± 1.0 mL) and 2 C (7.7 ± 0.8 mL) a continuously increased gassing was observed. Compared to literature (1.5 - 7.0 mL Ah^{-1})[34–36] the investigated cells produced 0.32 mL Ah^{-1} (0.1 C) up to 1.54 mL Ah^{-1} (2 C). The increase of C-rate and a reduction of total formation time resulted in more gas evolution during formation.

Nevertheless, the gas volume measured for the slowest 0.05 C (4.2 ± 0.8 mL) formation was also increased compared to the 0.1 C formation. Extended formation times can also lead to an increased electrolyte decomposition. An insufficient protection of electrolyte due to slow SEI formation leading to more unspecific gassing could be an explanation. Mao *et al.* suggested cells spent more time at low potentials which lead

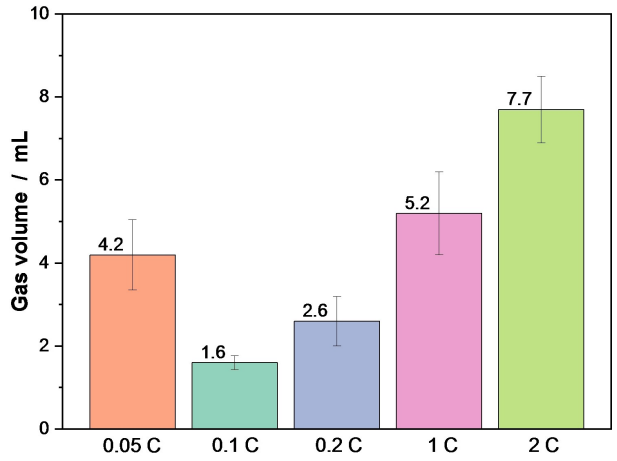

Figure 2. Gas volume increase in NMC622IIgraphite cells after formation with different C-rates. The error bars represent the deviation of gas evolution from three different cells.

to more parasitic reactions and following electrolyte decomposition.[26]

In Figure 3 a general relationship between gas volume and C-rate for the system is shown. The C-rate with most electrolyte protection is characterized by the lowest amount of gassing. It was suggested that a certain amount of specific gassing is necessary to build an effective SEI. In the following, the composition of the gassing is investigated to better understand the reasoning behind gassing.

2.2. Formation and Gas Composition Correlation

The quantification of the components in the formation gas was done *via* GC-BID and GC-TCD. The results are important to elucidate correlations in the gas composition between the formation procedures. Directly after formation, a small part of the gas phase was extracted using a direct sampling method, which was described in a previous publication.[45] The relative composition (V%) and the gas volume (mL) in the cell were correlated to calculate the total gas composition (mL) with respect to each analyte. Figure 4 shows the total amount of the gases in the cell. For the formation between 0.1 C–2 C only small amounts of H_2 were detected and the amount increased slightly with the C-rate. However, in case of the 0.05 C formation H_2 was identified as main component in the gas phase. H_2 can be formed during formation due to trace water reduction at the negative electrode.[25] But if there was a high amount of trace water in the electrolyte or the active materials in the cells were not free from humidity, the application of different C-rates should not have an effect on the water reduction and the same amount of H_2 would have been found in all other cells, too. Therefore, a high water content in the cells can be excluded. Metzger *et al.* identified protic electrolyte oxidation species from the positive electrode, which are reduced at the negative electrode, as the origin for increased H_2 evolution at high cell voltages.[25] Possibly, the slow SEI precipitation due to the slow potential decrease cannot protect these protic components from reduction at the graphite surface, which could cause the high amount of H_2 in the slow formation. H_2 was the significant difference in gassing behavior during 0.05 C formation. This could indicate a slow formation of SEI with accompanied parasitic reactions from species that diffuse from the cathode to the anode where they are reduced to H_2. The 0.1 C formation was probably fast enough to prevent this phenomenon. This supports the assumption of Metzger *et al.* that these species have to be built at the positive electrode (oxidation reaction) diffuse to the negative electrode and get reduced there.[25] Thus, these protic species can be reduced, if the SEI building is slower than the diffusion time between the electrodes. For this system, at C-rates lower than 0.1 C.

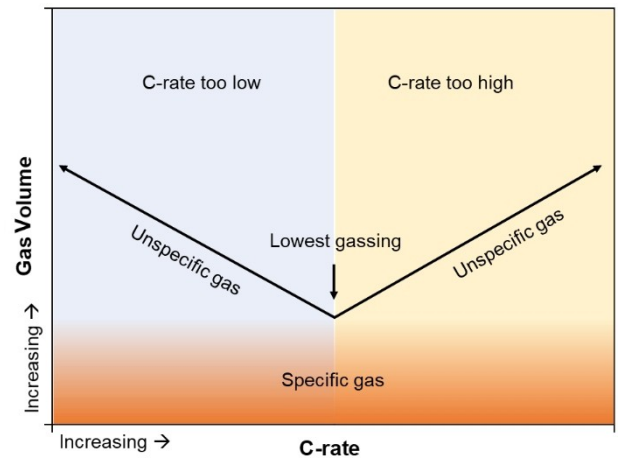

Figure 3. Scheme of the relationship between evolved gas volume and C-rate after formation. A formation with certain C-rate produces the smallest possible amount of gas which is required for SEI building (specific gas). Increasing or decreasing of C-rate results in more gassing due to unspecific reactions.

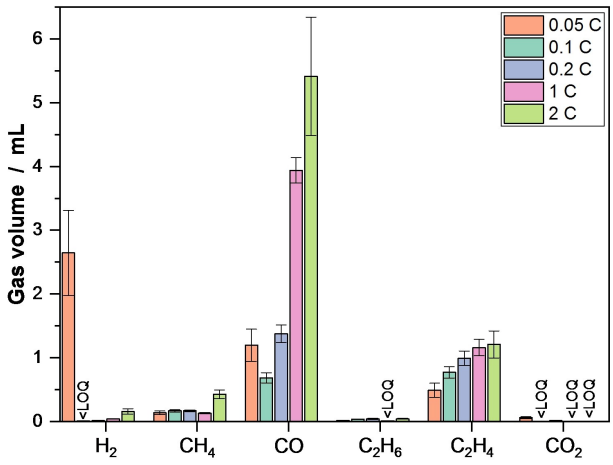

Figure 4. Total composition of the formation gas in NMC622IIgraphite cells after formation with different C-rates. The error results from the mean value of three cell volume measurements with associated standard deviation and the gas quantification with associated standard deviation from three measurements of each cell.

For the gases CH_4, C_2H_6, and CO_2 no significant interdependency on formation current was observed in the experiment. For the different formation procedures the composition results were in the same, low volume range compared to the other gases. An exception was a slightly higher signal for CH_4 at 2 C formation. In general, more CH_4 than C_2H_6 was detected in the gas phase. According to literature, the hydrocarbons mostly originate from the linear carbonates in the electrolyte mixture.[42,47–49]. Non or only traces of CO_2 were found in the cells after formation. CO_2 can be formed during formation but is known to be consumed at low potentials forming lithium oxalate.[50] Hence, it is plausible that most of the CO_2 was directly consumed and not detected in the gas phase after formation. However, also different results regarding CO_2 were mentioned in literature. High CO_2 contents were found after formation especially for VC containing electrolytes.[51,52] The origin of CO_2 can be Li_2CO_3 from the NMC material but also oxidative electrolyte decomposition reactions on the positive electrode as well as electrolyte reactions with HF.[48,49,53]

C_2H_4 is a well investigated electrolyte decomposition product, which is formed during formation of LIB cells. C_2H_4 can clearly be traced back to decomposition of the cyclic carbonate EC in a one or two electron reduction process.[23] Resulting solid products like Li_2CO_3 and $(CH_2OCO_2Li)_2$ are essential for the SEI formation.[42,54,55] Figure 4 demonstrates that the amount of C_2H_4 constantly increase with increasing C-rate. Accordingly, also an increased EC decomposition can be assumed. At high C-rates the relative increase gets smaller and flattens out.

The strongest effect of the C-rate was observed for the CO amount in the gas phase. CO was the main component of the formation gas mixture for all formation procedures except 0.05 C formation with higher H_2 volume. After 0.1 C formation a gas volume of 0.7 ± 0.1 mL and for 2 C, 5.4 ± 0.2 mL (factor of 7) was calculated for CO.

In literature the linear and cyclic solvents in the electrolyte were reported as origin of CO.[42,54,56–58] Therefore, the origin of the increased formation of CO during faster formation cannot clearly be assigned to a carbonate and further investigation has to be conducted. As described by the reactions in literature the electrochemical reactions resulting in the decomposition of carbonates are usually accompanied by the consumption of Li. The Li-ions are generally used to balance the charge of the reactions. Thus, increased specific gassing and SEI precipitation probably correlates with a more pronounced capacity decrease due to irreversible Li loss.

Figure 5 shows the capacity difference between the 0.1 C (5.9 Ah) and the 1 C (5.8 Ah) formation procedures from a second cycle with identical 0.1 C C-rate. The difference between both is ~2 % and therefore within the measuring error. Thus, a significant loss of capacity could not be observed, while more than three times the gas volume was determined (0.1 C vs. 1 C). Hence, the additional gassing cannot directly correlate to SEI formation and accompanied Li consumption. The additional amount of gas volume could therefore result from unspecific electrolyte decomposition. These decomposition pathways are usually not dependent on Li-ions as reactant and do not contribute to the SEI. Following the formation of SEI and consumption of Li is probably not depending on the C-rate. For a more intensive study of the formation process with different C-rates regarding the electrochemical performance, the reader is kindly referred to Münster et al.[29]

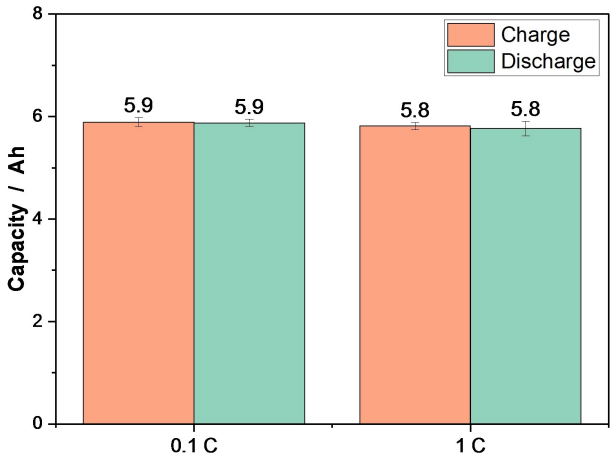

Figure 5. Comparison of charge and discharge capacity at 0.1 C after one formation cycle with 0.1 C and 1 C.

2.3. Electrolyte Investigation

The electrolyte contains VC as a film forming additive which is supposed to take part in the SEI-forming reaction. The exact influence of VC on the decomposition of the carbonates and SEI formation is still not clear. There are different reports how the VC molecules can interact with electrolyte and helps to form a proper SEI. On the one hand, it was reported that EC has a lower reduction potential than VC, hence VC decomposes before EC and protects EC during formation.[59–61] On the other hand, Wang *et al.* argue that VC acts as an anion intermediate and assists a controlled EC reduction.[62,63] In Figure 6 the quantification results of the extracted electrolyte using GC-FID

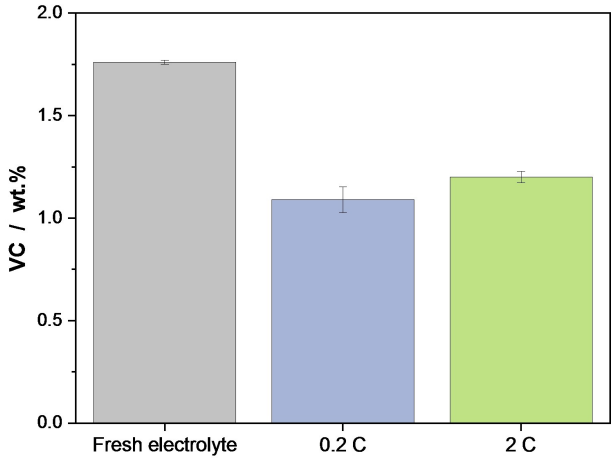

Figure 6. VC amount in wt.% for the fresh electrolyte and after formation with 0.2 C and 2 C.

after formation is illustrated. The VC amount in the electrolyte was reduced during formation. Nevertheless, during both procedures, VC has not been consumed completely, which is important to exclude reactions after a complete VC loss. The used solvent EMC is known to show transesterification reactions to DMC and DEC. VC as additive in the electrolyte, can strongly reduce the transesterification reaction also after formation.[64,65] Furthermore, decomposition of VC did not take place in unspecific gassing since the amount of consumed VC was similar for the tested C-rates.

2.4. Influence of the Graphite Material

The SEI is the interphase between the negative electrode and the electrolyte. Therefore, the characteristics of the graphite can affect the decomposition of electrolyte and the formation of the SEI. In order to investigate the influence of the graphite material on gassing in this cell system, a further graphite material (G II) was used as negative electrode material. Both specific surfaces of the graphite materials are similar. Therefore, the applied C-rates should not result in different current densities. In Figure 7 the difference in total gassing after formation with 0.2 C and 0.05 C compared to G I is shown. The total gas volume measured in the cells with G II under same electrochemical conditions was 6.1 ± 0.5 mL (0.2 C) and 4.8 ± 0.5 mL (0.05 C) and the standard system with G I 2.6 ± 0.6 mL (0.2 C) and 4.2 ± 0.9 mL (0.05 C). Here, it can be noticed, that the gassing behavior of G II is different compared to G I. For 0.05 C and 0.2 C H_2 formation is observed, which is not varying with C-rate and is less compared to G I at 0.05 C. Furthermore, significant amounts of CH_4 and a dependence of the C-Rate on the formation of CH_4 is present. The increase of total gas volume for a formation with 0.2 C by the factor of more than two in the cells with G II compared to G I is another significant difference, highlighting the impact of the graphite material on the gassing behavior. The graphite can have a significant influence on the decomposition reactions during formation.

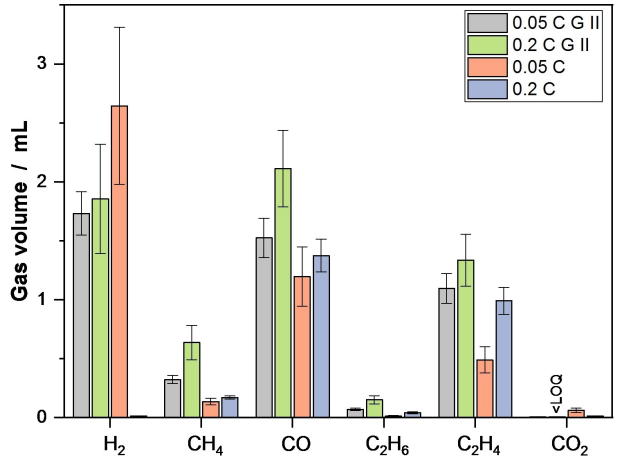

Figure 7. Influence of two different graphite materials on gassing after 0.05 and 0.2 C formation.

This also means that the morphology and composition of SEI can vary due to the amount of different precipitates available for the SEI. Especially, the reactions result in H_2 gassing seems to be affected by the graphite material. May there are different functional groups on the surface resulting in different reactions,.which has to be further investigated. The results show that it is essential to find the appropriate formation procedure for material combinations in LIBs.

3. Conclusions

In this work the effect of different C-rates on gas volume and gas composition were investigated in NMC622 II graphite LIBs. In all cells gassing was observed due to solvent molecule decomposition and resulting interphase formation. A differentiation between specific gassing due to interphase formation accompanied by Li consumption and unspecific gassing solely caused by solvent decomposition could be shown. It was assumed that the gas products are mainly formed by reactions that lead to the formation of the SEI. Increased gassing was observed for formation procedures with C-rates > 0.1 C, caused by an increased unspecific electrolyte decomposition, which mainly result in CO and C_2H_4. Increased gassing was also observed for formation with C-rates < 0.1 C, also caused by an increased unspecific electrolyte decomposition, but in this case, it mainly results in H_2 gassing. Presumably, two different electrolytic decomposition processes were identified, both reach a minimum at a certain C-rate. Higher (increased CO and C_2H_4 gassing) and lower (increased H_2 gassing) C-rates result in more electrolyte decomposition and gas formation.

The decomposition of VC did not take place in unspecific gassing since the amount consumed was the same for the tested C-rates. However, a second graphite material showed a significant difference in gassing, C-rates of 0.2 C led to a comparably high amount of H_2 gassing. Further experiments will focus on the specific carbonate origin of the formation gas components and whether they result from reaction on the positive or negative electrode.

Besides the gassing, the overall formation is an important factor for the industrial cell production. No significant impact of formation C-rate on discharge capacity could be found. Hence higher C-rates during formation can be a reasonable approach to lower cell production cost.

Acknowledgements

The authors thank the German Federal Ministry of Education and Research (BMBF) for funding the projects OptiZellForm (03XP0071B) within the ProZell cluster and HIT-Cell (03XP0113E) within Batterie 2020. Open access funding enabled and organized by Projekt DEAL.

Conflict of Interest

The authors declare no conflict of interest.

Keywords: lithium-ion battery · solid-electrolyte interphase · cathode-electrolyte interphase · formation · gas analysis · gas chromatography-barrier discharge ionization detection · Archimedes principle

[1] H. J. Santner, C. Korepp, M. Winter, J. O. Besenhard, K.-C. Möller, *Anal. Bioanal. Chem.* **2004**, *379*, 266–271.
[2] P. Niehoff, S. Passerini, M. Winter, *Langmuir* **2013**, *29*, 5806–5816.
[3] P. Niehoff, M. Winter, *Langmuir* **2013**, *29*, 15813–15821.
[4] T. Placke, V. Siozios, S. Rothermel, P. Meister, C. Colle, M. Winter, *Z. Phys. Chem.* **2015**, *229*, 1451–1469.
[5] U. S. Vogl, S. F. Lux, P. Das, A. Weber, T. Placke, R. Kostecki, M. Winter, *J. Electrochem.* **2015**, *162*, A2281–A2288.
[6] Y. Qian, P. Niehoff, M. Börner, M. Grützke, X. Mönnighoff, P. Behrends, S. Nowak, M. Winter, F. M. Schappacher, *J. Power Sources* **2016**, *329*, 31–40.
[7] J. O. Besenhard, M. Winter, *Pure Appl. Chem.* **1998**, *70*, 603–608.
[8] M. S. Whittingham, *Chem. Rev.* **2004**, *104*, 4271–4301.
[9] D. L. Wood, J. Li, C. Daniel, *J. Power Sources* **2015**, *275*, 234–242.
[10] S. J. An, J. Li, Z. Du, C. Daniel, D. L. Wood, *J. Power Sources* **2017**, *342*, 846–852.
[11] H.-H. Lee, Y.-Y. Wang, C.-C. Wan, M.-H. Yang, H.-C. Wu, D.-T. Shieh, *J. Power Sources* **2004**, *134*, 118–123.
[12] K. Xu, *Chem. Rev.* **2014**, *114*, 11503–11618.
[13] B. Rowden, N. Garcia-Araez, *Energy Rep.* **2020**, *6*, 10–18.
[14] Y. P. Stenzel, F. Horsthemke, M. Winter, S. Nowak, *Separations* **2019**, *6*, 26.
[15] R. Schmuch, R. Wagner, G. Hörpel, T. Placke, M. Winter, *Nat. Energy* **2018**, *3*, 267–278.
[16] R. W. Schmitz, P. Murmann, R. Schmitz, R. Müller, L. Krämer, J. Kasnatscheew, P. Isken, P. Niehoff, S. Nowak, G.-V. Röschenthaler, N. Ignatiev, P. Sartori, S. Passerini, M. Kunze, A. Lex-Balducci, C. Schreiner, I. Cekic-Laskovic, M. Winter, *Prog. Solid State Chem.* **2014**, *42*, 65–84.
[17] K. Xu, *Chem. Rev.* **2004**, *104*, 4303–4418.
[18] I. Cekic-Laskovic, N. von Aspern, L. Imholt, S. Kaymaksiz, K. Oldiges, B. R. Rad, M. Winter, *Top. Curr. Chem.* **2017**, *375*, 1–64.
[19] M. Winter, *Z. Phys. Chem.* **2009**, *223*, 1395–1406.
[20] S. J. An, J. Li, C. Daniel, D. Mohanty, S. Nagpure, D. L. Wood, *Carbon* **2016**, *105*, 52–76.
[21] J. Henschel, C. Peschel, S. Klein, F. Horsthemke, M. Winter, S. Nowak, *Angew. Chem. Int. Ed.* **2020**, *59*, 6128–6137; *Angew. Chem.* **2020**, *132*, 6184–6193.
[22] V. A. Agubra, J. W. Fergus, *J. Power Sources* **2014**, *268*, 153–162.
[23] C. Peschel, F. Horsthemke, M. Leißing, S. Wiemers-Meyer, J. Henschel, M. Winter, S. Nowak, *Batteries & Supercaps* **2020**, *3*, 1183–1192; Supercaps **2020**, 3, 1183–1192.
[24] J. B. Goodenough, Y. Kim, *Chem. Mater.* **2010**, *22*, 587–603.
[25] M. Metzger, B. Strehle, S. Solchenbach, H. A. Gasteiger, *J. Electrochem.* **2016**, *163*, A798–A809.
[26] C. Mao, S. J. An, H. M. Meyer, J. Li, M. Wood, R. E. Ruther, D. L. Wood, *J. Power Sources* **2018**, *402*, 107–115.
[27] S. Bhattacharya, A. T. Alpas, *Carbon* **2012**, *50*, 5359–5371.
[28] S. Bhattacharya, A. R. Riahi, A. T. Alpas, *MRS Proc.* **2012**, *1388*, 17.
[29] P. Münster, M. Diehl, J. E. Frerichs, M. Börner, M. R. Hansen, M. Winter, P. Niehoff, *J. Power Sources* **2021**, *484*, 229306.
[30] H. Maleki Kheimeh Sari, X. Li, *Adv. Energy Mater.* **2019**, *9*, 1901597.
[31] T. Minato, T. Abe, *Prog. Surf. Sci.* **2017**, *92*, 240–280.
[32] X. Yu, A. Manthiram, *Energy Environ. Sci.* **2018**, *11*, 527–543.
[33] C. P. Aiken, J. Xia, D. Y. Wang, D. A. Stevens, S. Trussler, J. R. Dahn, *J. Electrochem.* **2014**, *161*, A1548–A1554.
[34] C. P. Aiken, J. Self, R. Petibon, X. Xia, J. M. Paulsen, J. R. Dahn, *J. Electrochem.* **2015**, *162*, A760–A767.
[35] C. Mao, R. E. Ruther, L. Geng, Z. Li, D. N. Leonard, H. M. Meyer, R. L. Sacci, D. L. Wood, *ACS Appl. Mater. Interfaces* **2019**, *11*, 43235–43243.
[36] J. Self, C. P. Aiken, R. Petibon, J. R. Dahn, *J. Electrochem.* **2015**, *162*, A796–A802.
[37] H. Yoshida, T. Fukunaga, T. Hazama, M. Terasaki, M. Mizutani, M. Yamachi, *J. Power Sources* **1997**, *68*, 311–315.
[38] R. Petibon, L. M. Rotermund, J. R. Dahn, *J. Power Sources* **2015**, *287*, 184–195.
[39] C. R. Yang, Y. Y. Wang, C. C. Wan, *J. Power Sources* **1998**, *72*, 66–70.
[40] L. Madec, R. Petibon, K. Tasaki, J. Xia, J.-P. Sun, I. G. Hill, J. R. Dahn, *Phys. Chem. Chem. Phys.* **2015**, *17*, 27062–27076.
[41] L. D. Ellis, J. P. Allen, L. M. Thompson, J. E. Harlow, W. J. Stone, I. G. Hill, J. R. Dahn, *J. Electrochem. Soc.* **2017**, *164*, A3518–A3528.
[42] H. Ota, Y. Sakata, A. Inoue, S. Yamaguchi, *J. Electrochem.* **2004**, *151*, A1659–A1669.
[43] R. Nölle, K. Beltrop, F. Holtstiege, J. Kasnatscheew, T. Placke, M. Winter, *Mater. Today* **2020**, *32*, 131–146.
[44] F. Horsthemke, V. Winkler, M. Diehl, M. Winter, S. Nowak, *Energy Technol.* **2020**, *8*, 2070023.
[45] M. Leißing, M. Winter, S. Wiemers-Meyer, S. Nowak, *J. Chromatogr. A* **2020**, *1622*, 461122.
[46] L. Terborg, S. Weber, S. Passerini, M. Winter, U. Karst, S. Nowak, *J. Power Sources* **2014**, *245*, 836–840.
[47] G. Gachot, P. Ribière, D. Mathiron, S. Grugeon, M. Armand, J.-B. Leriche, S. Pilard, S. Laruelle, *Anal. Chem.* **2011**, *83*, 478–485.
[48] S. Leroy, F. Blanchard, R. Dedryvère, H. Martinez, B. Carré, D. Lemordant, D. Gonbeau, *Surf. Interface Anal.* **2005**, *37*, 773–781.
[49] S. Leroy, H. Martinez, R. Dedryvère, D. Lemordant, D. Gonbeau, *Appl. Surf. Sci.* **2007**, *253*, 4895–4905.
[50] K. Xu, A. von Cresce, *J. Mater. Chem.* **2011**, *21*, 9849.
[51] B. Strehle, S. Solchenbach, M. Metzger, K. U. Schwenke, H. A. Gasteiger, *J. Electrochem.* **2017**, *164*, A2513–A2526.
[52] K. U. Schwenke, S. Solchenbach, J. Demeaux, B. L. Lucht, H. A. Gasteiger, *J. Electrochem.* **2019**, *166*, A2035–A2047.
[53] T. Hatsukade, A. Schiele, P. Hartmann, T. Brezesinski, J. Janek, *ACS Appl. Mater. Interfaces* **2018**, *10*, 38892–38899.
[54] M. Onuki, S. Kinoshita, Y. Sakata, M. Yanagidate, Y. Otake, M. Ue, M. Deguchi, *J. Electrochem.* **2008**, *155*, A794–A797.
[55] D. Aurbach, B. Markovsky, I. Weissman, E. Levi, Y. Ein-Eli, *Electrochim. Acta* **1999**, *45*, 67–86.
[56] F. Wang, F. Varenne, D. Ortiz, V. Pinzio, M. Mostafavi, S. Le Caër, *ChemPhysChem* **2017**, *18*, 2799–2806.
[57] R. Mogi, M. Inaba, Y. Iriyama, T. Abe, Z. Ogumi, *J. Power Sources* **2003**, *119–121*, 597–603.
[58] W. Kong, H. Li, X. Huang, L. Chen, *J. Power Sources* **2005**, *142*, 285–291.
[59] K. Tasaki, K. Kanda, T. Kobayashi, S. Nakamura, M. Ue, *Electrochim. Acta* **2006**, *153*, A2192–A2197.
[60] S. Yoon, H. Kim, J.-J. Cho, Y.-K. Han, H. Lee, *J. Power Sources* **2013**, *244*, 711–715.
[61] H. M. Jung, S.-H. Park, J. Jeon, Y. Choi, S. Yoon, J.-J. Cho, S. Oh, S. Kang, Y.-K. Han, H. Lee, *J. Mater. Chem. A* **2013**, *1*, 11975–11981.
[62] Y. Wang, S. Nakamura, M. Ue, P. B. Balbuena, *J. Am. Chem. Soc.* **2001**, *123*, 11708–11718.
[63] Y. Wang, S. Nakamura, K. Tasaki, P. B. Balbuena, *J. Am. Chem. Soc.* **2002**, *124*, 4408–4421.
[64] L. Madec, R. Petibon, K. Tasaki, J. Xia, J.-P. Sun, I. G. Hill, J. R. Dahn, *Phys. Chem. Chem. Phys.* **2015**, *17*, 27062–27076.
[65] R. Petibon, J. Xia, J. C. Burns, J. R. Dahn, *J. Electrochem. Soc.* **2014**, *161*, A1618–A1624.

Manuscript received: February 25, 2021
Revised manuscript received: March 30, 2021
Accepted manuscript online: April 27, 2021
Version of record online: May 14, 2021